Available online at www.sciencedirect.com
SCIENCE DIRECT®
Acta Materialia 52 (2004) 2229–2238
Acta MATERIALIA
www.actamat-journals.com

Orientation dependence of nanoindentation pile-up patterns and of nanoindentation microtextures in copper single crystals

Y. Wang, D. Raabe *, C. Klüber, F. Roters

Microstructure Physics, Max-Planck-Institut für Eisenforschung, Max-Planck-Strasse 1, 40237 Düsseldorf, Germany

Received 6 March 2003; received in revised form 20 August 2003; accepted 12 January 2004

Abstract

We present a study about the dependence of nanoindentation pile-up patterns and of microtextures on the crystallographic orientation using high purity copper single crystals. Experiments were conducted on a Hysitron nanoindentation setup using a conical indenter in order to avoid symmetries others than those of the crystal structure. Orientation measurements were conducted using a high resolution electron back-scatter diffraction technique for the automated acquisition of texture mappings around the indents. Simulations were carried out by means of a 3D elastic–viscoplastic crystal plasticity finite element method which takes full account of crystallographic slip and orientation changes during indentation. The experiments as well as the simulations show that the pile-up patterns on the surfaces of (0 0 1)-, (0 1 1)- and (1 1 1)-oriented single crystals have four-, two-, and sixfold symmetry, respectively. The different pile-up patterns can be explained in terms of the strong crystallographic anisotropy of the out-of-plane displacements around the indents. Pronounced accumulation of material entailing characteristic pile-up patterns occurs along the intersection vectors between the primary crystallographic slip planes and the indented surface planes.

Keywords: Texture; Nanoindentation; Plastic deformation; Copper; Single crystal; Pile-up

1. Introduction

An important feature of indentation experiments is that the material around the contact area tends to deform upwards (pile-up) or downwards (sink-in) with respect to the indented surface plane. The occurrence of such pile-up and sink-in patterns is usually interpreted in terms of the strain-hardening behavior of the indented material [1–4]. According to these studies the surface around indents tends to pile up against the indenter in cases where the indented sample is heavily pre-strained with only little reserves for further work-hardening or has generally a low strain-hardening potential. On the other hand, when the sample is fully annealed and has a high strain-hardening potential, the surface around indents tends to sink in e.g. [1–4].

The reason for this relationship between strain hardening behavior and displacement patterns is plausible: well-annealed soft metals which exhibit a high strain-hardening rate tend to show far off field plasticity yielding a large lateral smear out of the plastic out-of-plane displacement field. Rapid strain-hardening in the immediate vicinity of the indenter tip will cause plastic deformation to occur gradually further away from the contact region, causing the material to be displaced far away from the indentation entailing sink-in patterns. In contrast, strain-hardened materials as well as alloys and metallic glasses which exhibit a low (residual) strain-hardening rate will reveal a stronger localization of the plastic zone, creating a local pile-up instead of a sink-in displacement pattern around the indent.

The situation is somewhat less clear for nanoindented single crystals. Various authors who reported about such experiments [5–10] observed that for most annealed single-crystals, such as Cu, W, Fe, Al, or NiAl, distinct pile-up patterns occur only in certain directions around the indentation depending on the crystallographic

* Corresponding author. Tel.: +49-211-679-2278; fax: +49-211-679-2333.
E-mail address: raabe@mpie.de (D. Raabe).

1359-6454/$30.00 © 2004 Acta Materialia Inc. Published by Elsevier Ltd. All rights reserved.
doi:10.1016/j.actamat.2004.01.016

orientation of the single-crystal [5–10]. Very detailed atomistic simulations about the incipient stages of nanoindentation in face centered cubic single crystals were recently conducted by Li et al. [11] and Van Vliet et al. [12]. These studies provided excellent insight into the early stages of nucleation of slip during the beginning of indentation. The data revealed a strong influence of the crystallography on the formation of surface patterns.

Good knowledge of the deformation zone around an indent is of considerable importance for nanoindentation testing because the shape of the out-of-plane displacement zone determines the actual contact area between the indenter and the specimen. Sink-in patterns reduce and pile-up patterns increase the contact area. These differences in the surface deformation mode affect the quantitative analysis of the hardness measurements. Not taking the piling-up or sinking-in into account in micro- and nanoindentation hardness tests can result in significant errors when extracting hardness values from the experimental data [1,2].

The current investigation is concerned with the anisotropy of the surface profiles around nanoindents and their crystallographic interpretation in terms of the active slip systems and local texture changes. Our approach to this issue consists in a combination of indentation testing, high-resolution texture measurements, and simulations. For the experiments we use single crystalline copper specimens with different orientations. The indentation tests are conducted with a Hysitron *TriboIndenter* setup using a conical indenter in order to avoid symmetries others than those of the crystal structure. Texture measurements are performed using a high resolution electron back-scatter diffraction (EBSD) technique for the automated acquisition of texture mappings around the indents. The experimentally observed nanoindentation pile-up patterns and textures are compared to corresponding predictions obtained by a 3D crystal plasticity finite element simulation method which takes full account of crystallographic slip and orientation changes during indentation.

2. Experimental procedure

2.1. Nanoindentation setup

The experiments were carried out with a Hysitron nanoindenter system (*TriboIndenter*). The instrument includes a XYZ-sample-stage and a setup which combines a piezo-scanner as known from conventional atomic force microscopy (AFM) with a transducer and a diamond indenter-tip. The XYZ-stage is used to position the sample under the piezo scanner, which then conducts the fine positioning as well as the approach of the indenter in normal direction. A three-plate capacitor (transducer) with the indenter fixed to the middle plate is being used to move the indenter tip in normal direction by applying a bias DC voltage on the bottom plate of the capacitor. The electric field potential between the plates varies linearly with the displacement of the indenter and the middle plate is attached to in normal direction. In this way the displacement of the indenter can be measured accurately. Once the indenter tip is positioned on top of the sample, it can either be forced into the sample by applying a bias voltage on to the bottom capacitor of the transducer (hardness test) or it can be moved in lateral direction (x–y-plane) with help of the piezo controller to image the sample surface comparable to an conventional atomic force microscope.

2.2. Hardness testing procedure and indenter area function

The nanohardness tests were conducted in load-controlled mode. In this mode the force is translated into a bias DC voltage on the lower capacitor plate continuously during the indentation experiment. The displacement of the indenter is measured simultaneously to give a force–displacement curve.

To calculate both, hardness and Young's modulus accurately from the force–displacement data, it is necessary to know the exact geometry of the indenter tip. Therefore the indenter cross-section area function is obtained by performing indentation tests of different indentation depths into a material with a known and constant Young's modulus (in this and most other cases reported in the literature this is done with quartz).

For each of these indents a power law for the force, P, is fitted to the unloading curve of the experiment using the empirical approach

$$P = b \cdot (h - h_{\mathrm{f}})^k, \tag{1}$$

where h and h_{f} are the indenter displacements at maximum load and after unloading, respectively, and b and k are constants. From this approximation and the known indentation depth at maximum load, the stiffness, S, at the point of unloading

$$S = \frac{\mathrm{d}P}{\mathrm{d}h} = \frac{2}{\sqrt{\pi}} E_{\mathrm{r}} \sqrt{A_{\mathrm{c}}}, \tag{2}$$

and thus the contact area A_{c} of the indenter can be recalculated according to

$$A_{\mathrm{c}} = \frac{\pi}{4} \frac{1}{E_{\mathrm{r}}^2} \frac{1}{(C - C_f)^2}, \tag{3}$$

in which E_{r} is the reduced modulus of the sample material, and C and C_{f} are the total and the frame compliance, respectively. Plotting the area, A, over the

indentation depth gives the necessary geometry of the indenter. From the so obtained data set an area function of the form given below can be obtained by a fitting procedure

$$A = 24, \quad 5h_c^2 + C_1 h_c^1 + C_2 h_c^{\frac{1}{2}} + C_3 h_c^{\frac{1}{4}} + \cdots + C_8 h_c^{\frac{1}{128}}, \qquad (4)$$

with the contact depth h_c and the fit constants C_1 through C_8.

2.3. Sample preparation and experiments

A copper single crystal was drawn from the melt and cut into four samples with cubic shape by spark erosion to give {1 0 0}-,{1 1 0}-, and {1 1 1}-oriented surface planes. The surface planes were wet-ground, diamond-polished, and finally electro-polished. Orientation mappings were conducted using an scanning electron microscope equipped with EBSD technology. Nanoindentation experiments were performed on all above orientations. Between 20 and 35 indentation test of different maximum indentation depths between 10 and 250 nm were performed and both, hardness and Young's modulus were calculated for each of them. AFM images of relatively large indents of diameter of 3–5 μm were taken.

3. Simulation procedure

3.1. Crystal plasticity constitutive model

The single-crystal plasticity constitutive model used for the finite element simulations conducted for this study has been formulated in accord with the recent work of Kalidindi et al. [13–16] which is formulated on the basis of earlier pioneering work in this field by the groups of Lee, Rice, Hill, Asaro, Peirce, and Needleman [17–22]. In the following we briefly summarize its essential ingredients.

For finite deformation, the total deformation gradient, $\mathbf{F}$, mapping a reference configuration of the material to the deformed configuration, can be multiplicatively decomposed into elastic and plastic components as

$$\mathbf{F} = \mathbf{F}^e \mathbf{F}^p, \qquad (5)$$

where $\mathbf{F}^p$, describing deformation gradients due to plastic deformation alone, maps neighborhoods of the original configuration to an intermediate configuration. $\mathbf{F}^e$, containing deformation gradients due to both elastic stretching as well as the lattice rotation, maps neighborhoods of the intermediate configuration to the deformed configuration. With plastic deformation, $\mathbf{F}^p$ evolves according to the flow rule

$$\dot{\mathbf{F}}^p = \mathbf{L}^p \mathbf{F}^p, \qquad (6)$$

with $\mathbf{L}^p$ being the plastic flow rate. In crystals, $\mathbf{L}^p$ is composed of the superposition of the resolved crystallographic plastic shear rates, $\dot{\gamma}^\alpha$, such that

$$\mathbf{L}^p = \sum_\alpha \dot{\gamma}^\alpha \mathbf{S}_0^\alpha, \quad \mathbf{S}_0^\alpha = \mathbf{m}_0^\alpha \otimes \mathbf{n}_0^\alpha, \qquad (7)$$

in which $\dot{\gamma}^\alpha$ is the shearing rate on the slip system α, and $\mathbf{m}_0^\alpha$ and $\mathbf{n}_0^\alpha$ denote the slip direction and the slip plane normal of the slip system, respectively, in the initial unloaded configuration. The shearing rate on the each slip system depends on the resolved shear τ^α and the slip resistance s^α of that slip system and it is taken as

$$\dot{\gamma}^\alpha = \dot{\gamma}_0 \left| \frac{\tau^\alpha}{s^\alpha} \right|^{1/m} \operatorname{sign}(\tau^\alpha), \qquad (8)$$

in which $\dot{\gamma}_0$ denotes a reference value of the slip rate and m represents the strain rate sensitivity parameter. In the present study, $\dot{\gamma}_0$ is taken as 0.001 s^{-1} and m is taken as 0.05. The evolution of the slip system resistance can be taken as

$$\dot{s} = \sum_\beta h^{\alpha\beta} \left| \dot{\gamma}^\beta \right|, \quad h^{\alpha\beta} = q^{\alpha\beta} h^{(\beta)}, \quad h^{(\beta)} = h_0 \left\{ 1 - \frac{s^\beta}{s_s} \right\}^a, \qquad (9)$$

where $q^{\alpha\beta}$ are the components of a matrix which describe the latent hardening behavior of the crystal, and h_0, a and s_s are slip system hardening parameters which are taken to be identical for all slip systems. For the 12 $\{1\,1\,1\}\langle 1\,1\,0\rangle$ slip systems of an fcc crystal, we take $q^{\alpha\beta} = 1.0$ if the slip systems α and β are coplanar and $q^{\alpha\beta} = 1.4$ if they are not coplanar. For the indented material (single-crystalline copper), the values of the slip system hardening parameters h_0, a, s_s, and the initial value of the slip resistance s_0 are taken to be $h_0 =$ 180 MPa, $s_s = 148$ MPa, $a = 2.25$, and $s_0 = 16$ MPa. An elastic strain measure, $\mathbf{E}^e$, corresponding to the Cauchy–Green strain with respect to the intermediate configuration, is defined as

$$\mathbf{E}^e \equiv (1/2)\left\{ \mathbf{F}^{eT} \mathbf{F}^e - \mathbf{I_2} \right\}, \qquad (10)$$

with $\mathbf{I_2}$ being the second-order identity tensor. The stress measure, $\bar{\mathbf{T}}$, is related to the Cauchy stress, T, through the transformation

$$\bar{\mathbf{T}} = \det(\mathbf{F}^e) \mathbf{F}^{e-1} \mathbf{T} \mathbf{F}^{e-T}. \qquad (11)$$

Stress is related to elastic strain by

$$\bar{\mathbf{T}} = \mathbf{L}[\mathbf{E}^e], \qquad (12)$$

where $\mathbf{L}$ is the fourth-order elasticity tensor. The elasticity tensor $\mathbf{L}$ for a face centered cubic crystal requires three material parameters C_{11}, C_{12}, and C_{44}, which for copper are taken to be $C_{11} = 168.0$ GPa, $C_{12} = 121.4$ GPa, and $C_{44} = 75.4$ GPa.

The constitutive law described above requires some comments with respect to the fact that we apply it to the prediction of nanoindentation. Before conducting crystal plasticity finite element simulations it must be

considered that the deformation is often found to be more or less discrete and jumpy instead of continuous when the indentation depth is below about 50–100 nm. Also, in such cases the mechanical size-effect may play a substantial role in copper which would suggest to use an altered hardening law including the nanoscale size dependence of hardness.

However, in cases where the indentation depth is very large, as in the experiments we study in this work (our experiments are given for 250 nm indentation depth and indentation diameters of 3000–5000 nm), the depth–load curve shows an asymptotic behavior. Plastic flow in this regime is no longer jerky and the mechanical size effect does no longer play a substantial role. This means the simulations in this study can serve to investigate the limits of the validity of conventional viscoplastic hardening laws which work without the explicit consideration of size effects at small scale plasticity.

Besides this mechanical aspect our study concentrates more on the crystallographic evolution of the surface patterns surrounding the indents as well as on the microtexture development in this regime rather than on the early stages of the process.

3.2. Finite element implementation

The constitutive model for single-crystalline copper described above and the associated implicit time-integration procedure proposed by Kalidindi et al. [16] were implemented into the commercial finite element code MARC by means of the user defined material subroutine HYPELA2 [23].

The three-dimensional finite element mesh is shown in Fig. 1. The mesh was carefully refined in the contact region. A set of 2780 eight-node brick elements was used to discretize the sample. The elements used an assumed strain formulation to improve the bending behavior. The indenter tip was modeled as a rigid conical tool with a spherical tip. The simulations were conducted on three crystallographic orientations (0 0 1), (0 1 1), and (1 1 1) of single crystalline copper with anisotropic elastic–viscoplastic properties.

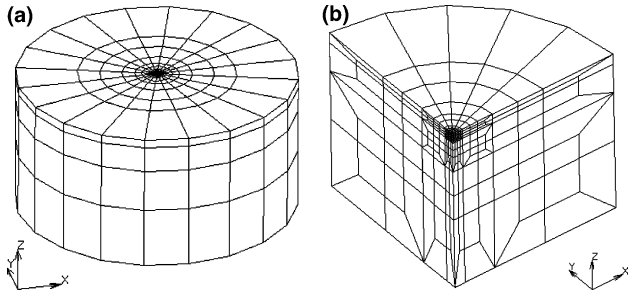

Fig. 1. The mesh used for the finite element discretization of the nanoindentation simulation: (a) outside view on the mesh and (b) a quarter of the mesh revealing the discretization around the indent area.

In order to investigate the influence of friction in the context of Coulomb's linear law on the predictions we conduced first a set of simulations with different friction coefficients ranging from $\mu = 0.0$ to 0.3. We observed that the predicted stress and strain fields were nearly independent of the friction conditions [24,25]. Consequently, we assumed a friction coefficient of 0 between the indenter and the sample in the finite element predictions described below to save computing time.

While the stress–strain-fields obtained by J2-based isotropic continuum predictions of plastic forming typically reveal a strong dependence on friction, it is often found that this dependence is much less pronounced when using discrete crystal plasticity constitutive approaches [26]. Dève et al. [27] and Harren and Asaro [28] already pointed out that nonuniform deformation and strain localization which are usually taken as characteristic symptoms of a pronounced influence of friction arise anyway quite naturally in crystalline matter as a consequence of the reduction in the degrees of freedom of material flow to crystallographic shear.

4. Results and discussion

4.1. Crystal mechanics

The finite element calculations show different surface profiles around the simulated indents for the three different surface orientations. Fig. 2 shows the simulated contour plots of the out-of-plane displacement profiles on the surfaces of the (0 0 1)-, (0 1 1)- and (1 1 1)-oriented surfaces. The data reveal fourfold symmetry of the height profile for the (0 0 1)-oriented crystals, twofold symmetry for the (0 1 1)-oriented crystals, and sixfold symmetry for the (1 1 1)-oriented crystals, respectively.

Experimental nanoindentation tests on the same crystallographic surfaces of single-crystal copper samples were performed using a Hysitron *TriboIndenter*. Fig. 3 shows AFM images of the pile-up patterns on the different surfaces after indentation. The experimental and simulated displacement patterns reveal excellent agreement, i.e. the profile around the indent on the (0 0 1)-oriented crystal reveals fourfold symmetry, for the (0 1 1)-oriented crystal twofold symmetry, and for the (1 1 1)-oriented crystal sixfold symmetry. The difference in absolute numbers for the profile heights between the simulations and the experiments is due to the scaling of the calculations which enters through the curvature of the indenter tip.

Fig. 4 shows the simulated in-depth lateral distribution of the displacement field for the three different single crystals. The gray scale levels are the same as in Fig. 2. Fig. 5 shows corresponding sections through the simulated 3D samples. The data reveal in all three cases pile-up rather than sink-in behavior. However, piling up

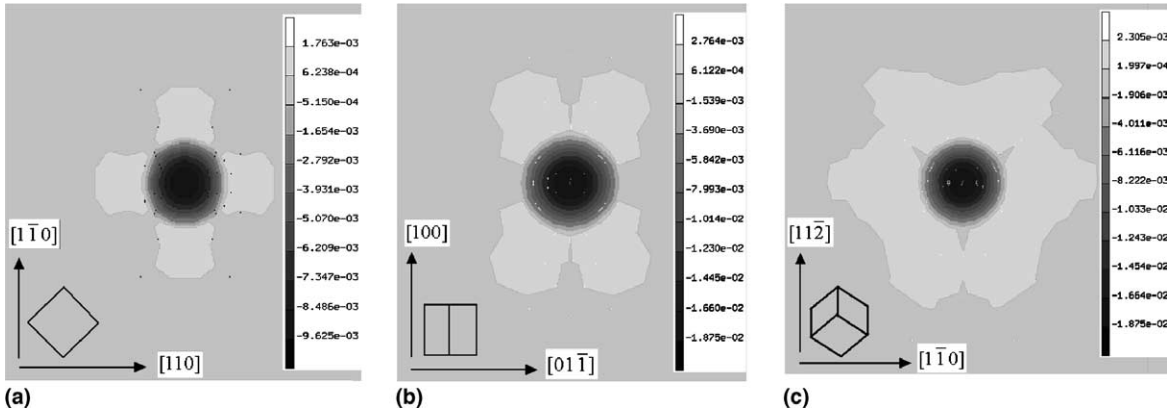

Fig. 2. Simulated contour plots showing the out-of-plane displacement profiles on (a) (0 0 1), (b) (0 1 1) and (c) (1 1 1) oriented copper single crystal surfaces after indentation with a conical indenter. The displacements are given in units of mm where the scaling enters through the curvature of the indenter tip.

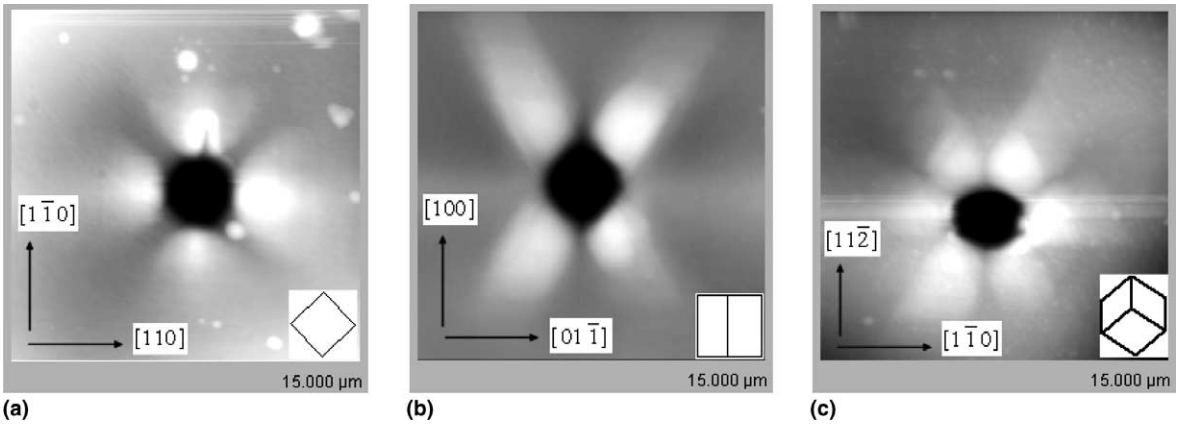

Fig. 3. Experimentally observed contour plots of the pile-up patterns on (a) (0 0 1), (b) (0 1 1) and (c) (1 1 1) oriented copper single crystal surfaces after indentation with a conical indenter. The difference between the two extrema (indicated here by black and white) amounts to 250 nm. The gray scaling between the two extrema is linear.

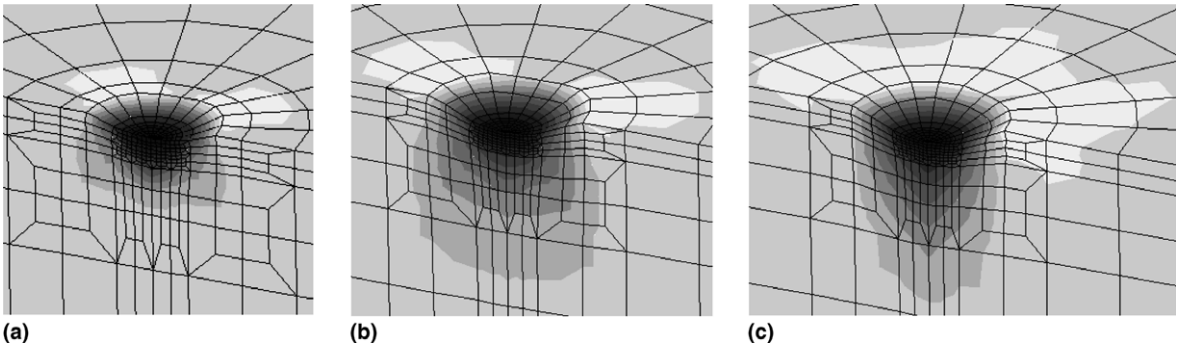

Fig. 4. 3D cuts through the simulated indents: (a) (0 0 1), (b) (0 1 1) and (c) (1 1 1) oriented surfaces of copper single crystals after indentation with a conical indenter. The corresponding gray scale levels are the same as in Fig. 2.

occurs only in well defined limited zones around the indents, i.e. the pile-up patterns are strictly crystallographic and orientation dependent.

Earlier studies about the relationship between the plastic properties and the surface shapes around the indents suggested that the pile-up or respectively sink-in behavior around indents is primarily affected by the strain-hardening rate of the indented material [1–3]. It was suggested that soft metals which have a high plastic strain-hardening rate and sufficient hardening reserves

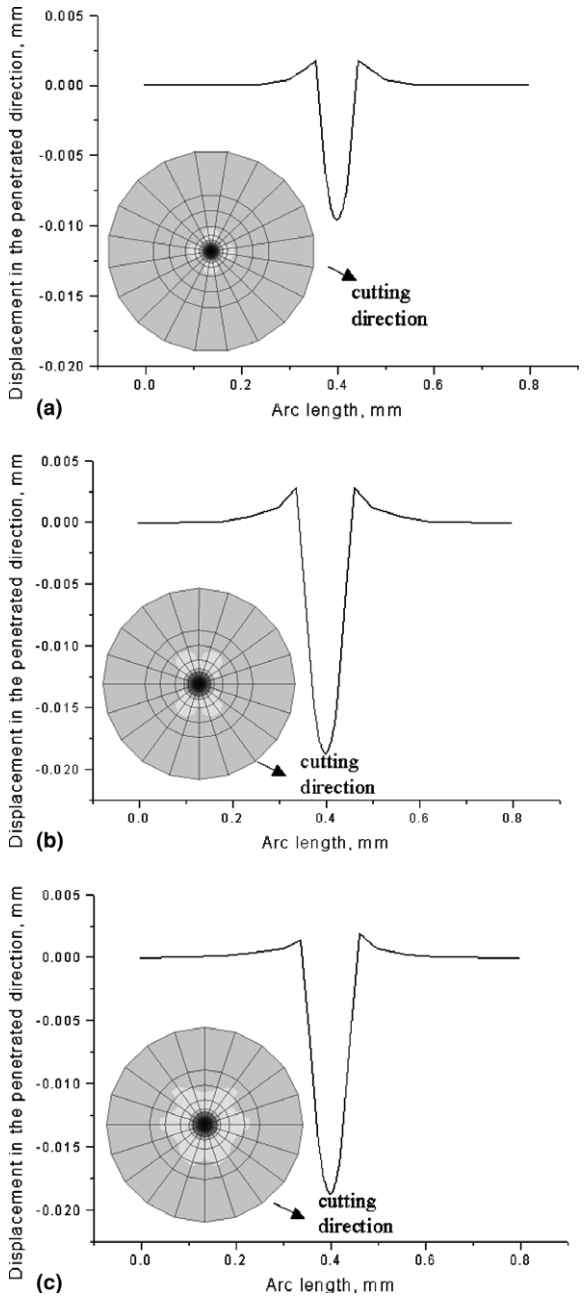

Fig. 5. Height profiles in the form of 3D cuts through the simulated indents: (a) (0 0 1), (b) (0 1 1) and (c) (1 1 1) oriented surfaces of copper single crystals after indentation with a conical indenter.

tend to show a large lateral smear out of the plastic displacement field. In this picture it is assumed that rapid strain-hardening around an indent carries the plastic deformation zone gradually further away from the contact region. This would entail sink-in patterns in the vicinity of the contact area. In contrast, strain-hardened materials as well as alloys and metallic glasses which exhibit a low (residual) strain-hardening reserve are assumed to reveal plastic localization in the immediate vicinity of the contact zone. Such constitutive behavior is assumed to produce pile-up instead of sink-in patterns around an indent.

Our current experimental and simulation data are at first sight not fully consistent with this classical picture. Similar observations of pile-up instead of sink-in patterns around nanoindents in poly- and single-crystalline copper specimens were also earlier reported by McElhaney et al. [29], by Lim and Chaudhri [30–32], and by Lui and Ngan [33]. Figs. 2–5 show two important facts in this context. First, the different patterns are strongly related to the indented crystallographic planes. Second, the patterns are all pile-up and not sink-in patterns, although piling up occurs only in well defined areas which reveal a strictly crystallographic pile-up shape characteristic of the indented plane. These two observations seem to contradict some aspects of the current understanding of indent plasticity since we used undeformed soft copper single crystals with considerable strain hardening reserves. Such constitutive behavior would suggest sink-in patterns rather than pile-up patterns.

We, therefore, interpret the observed pile-up patterns in terms of the kinematics and dynamics associated with such highly localized and crystallographic plastic flow. By *kinematics* we mean that the geometry of the observed primary slip dominates the local deformation around the indents to such a large extent that the mere translation of material along a small set of active slip systems to the surface might dominate the pile-up behavior for simple geometrical reasons. As will be discussed in more detail below and as was shown by the crystal plasticity finite element analysis we can indeed confirm the assumption that a small set of primary slip systems carries the deformation process. This is also underlined by the highly crystallographic pile-up patterns which would be much more blurred in the case that substantial activity on secondary slip systems had occurred. By *dynamics* we mean that the activation of a small set of slip systems which carry most of the material translation without seeing much interaction with secondary slips might reveal rather small local strain hardening. In other words, parallel dislocation glide on a small number of active primary slip systems might locally lead to very small strain hardening rates. This means that one might be inclined to interpret the observed patterns in terms of highly localized microscopic strain hardening effects. In this picture one would attribute the observation that all patterns are pile-up rather than sink-in patterns to the crystallographic and locally parallel flow of material along small confined volumes which are essentially prescribed by the local orientation factors. This means that one must obviously take care before using bulk isotropic strain hardening criteria for the interpretation of pile-up patterns around conical indents. Such argumentation on the basis of the dominance of local crystallographic hardening mecha-

nisms as opposed to the global isotropic behavior is supported by the clear symmetry of the observed patterns as apparent in particular in Fig. 2 (simulation) and Fig. 3 (experiment).

At ambient temperature the active glide systems of copper (face centered cubic) consist of $\{1\,1\,1\}$ glide planes and $\langle 1\,1\,0\rangle$ slip directions. For the indented $(0\,0\,1)$ surface, the primary slip planes $(1\,\bar{1}\,1)$ and $(1\,1\,1)$ intersect the indented plane along the $[1\,1\,0]$ and $[1\,\bar{1}\,0]$ directions, Fig. 6(a). Since these two planes serve as primary glide planes for slip, i.e. for the crystallographic translation of material parallel to them, their activation naturally produces excess material along their intersection lines with the surface plane. This means that the surface around the indent must be elevated along the $[1\,1\,0]$ and $[1\,\bar{1}\,0]$ directions entailing a surface pattern with a fourfold in-plane symmetry owing to the crystallography of the two $\langle 1\,1\,0\rangle$ intersection vectors. This is exactly what we observed in the simulations (Fig. 2(a)) and in the experiments (Fig. 3(a)).

For the indented $(0\,1\,1)$ surface (Figs. 2(b) and 3(b)), the primary slip planes $(1\,\bar{1}\,1)$ and $(1\,1\,\bar{1})$ cross the indented plane along the two crystallographic directions $[2\,1\,\bar{1}]$ and $[2\,\bar{1}\,1]$ and, therefore, the pile-up pattern reveals a twofold symmetry. For the indented $(1\,1\,1)$ surface, the slip planes $(1\,1\,\bar{1})$, $(\bar{1}\,1\,1)$, and $(1\,\bar{1}\,1)$ intersect the indented plane along the three lines $[1\,\bar{1}\,0]$, $[0\,1\,\bar{1}]$, and $[1\,0\,\bar{1}]$, which entails sixfold in-plane symmetry.

In summary, we conclude that the patterns and their symmetries around the indents on the different crystallographic surfaces can be well understood in terms of material translation along the intersection vectors of the primary slip systems with the indented surface. The interpretation of the pile-up vs. sink-in behavior remains more speculative. Although we gave some thoughts about the dynamics associated with highly localized flow around the indents with respect to pile-up vs. sink-in patterning it must be noted that the analysis of the dominant crystallographic slips serves essentially to explain the deformation patterns and their in-plane symmetry rather than the actual pile-up vs. sink-in behavior.

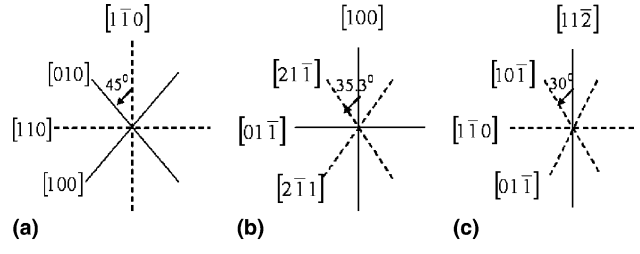

Fig. 6. Crystallography of the experimentally observed and simulated out-of-plane displacement profiles on (a) $(0\,0\,1)$, (b) $(0\,1\,1)$ and (c) $(1\,1\,1)$ oriented copper surfaces after indentation with a conical indenter.

4.2. Evolution of the crystallographic texture at the nanoindents

Fig. 7 shows the $(0\,0\,1)$ and $(0\,1\,1)$ pole figure projections of the crystallographic textures of the conical indents as predicted by the crystal plasticity finite element method. The two pole figures in each row on the left hand side show the single orientation data as collected from all modes and the two pole figures on the right hand side show the corresponding iso-pole-density plots. The pole figures comprise the complete simulated texture, i.e. they show all points around the indents and inside the indents. Fig. 7(a) shows the data for the $(0\,0\,1)$ oriented surface after indentation, Fig. 7(b) for the $(0\,1\,1)$ surface, and Fig. 7(c) for the $(1\,1\,1)$ surface.

For a correct interpretation of the pole figures it is important to note the respective reference systems given by the initial orientations of the single crystals prior to loading relative to their border coordinates (see small icons in the upper left corners of the pole figures). Table 1 gives the Euler angles reduced for cubic crystal symmetry and orthothropic sample symmetry for the three copper crystals prior to loading.

The simulated texture for the indent in the $(0\,0\,1)$ surface reveals strong rotations about the longitudinal axis and about the transverse axis. These two rotations can be readily understood in terms of the prevailing slip crystallography, even without considering the fine details of the finite element analysis. When we assume a simple compression state at the beginning of loading then the antisymmetric portions arising from the slip on the four dominating $\{1\,1\,1\}$ glide planes along the corresponding main slip directions may explain the observed spins (Fig. 8). A similar explanation holds for the interpretation of the texture scatter in Fig. 7(b) and (c), although the rotations about the sample normal direction in Fig. 7(b) do not fit into this simplistic picture.

Fig. 9 shows the lateral distribution of the misorientation fields around and below the indent. The indents were simulated on the $(1\,1\,1)$ oriented surface plane of a copper single crystal using a conical indenter (compare to Fig. 5(c)). The data are presented in the $(1\,\bar{1}\,0)$ crystallographic cutting plane. The color code shows the accumulated orientation change relative to the starting orientation. The reorientation axis is not given. The data points show strong re-orientation fields of up to 20° orientation deviation relative to their initial orientation. The cut reveals that the pronounced texture changes are accumulated particularly in two zones below the indenter (together with their respective symmetrically equivalent zones). The larger re-orientation areas (bright arrows) are located in the maximum shear zone at the rim of the indent in the $(1\,\bar{1}\,0)$ crystallographic plane. The smaller re-orientation areas (dark arrows) are located closer to the tip of the indenter. Basic considerations about the arrangement of geometrically necessary

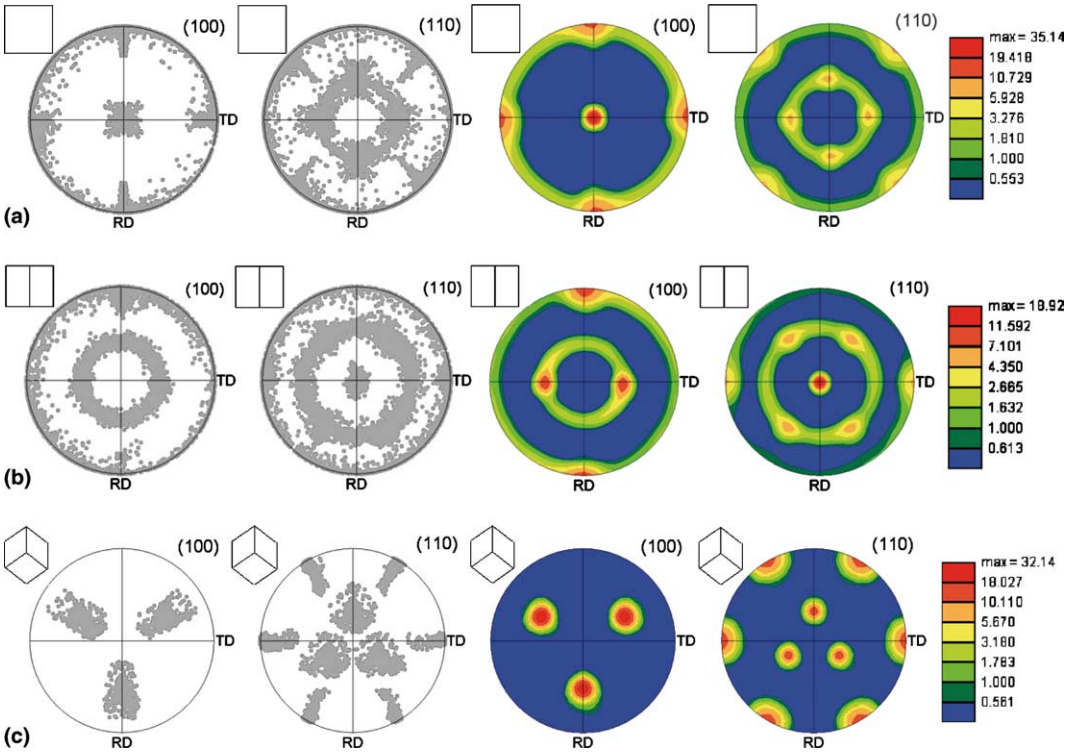

Fig. 7. (0 0 1) and (0 1 1) pole figures with single orientations (left hand side) and in the form of iso-pole-density plots (right hand side) for simulated textures. The pole figures show all points around the indent and inside the indent: (a) (0 0 1), (b) (0 1 1) and (c) (1 1 1) oriented surfaces after indentation (simulation).

Table 1
Euler angles of the three starting orientations

Orientation	φ_1 [°]	ϕ [°]	φ_2 [°]
(0 0 1)[1 0 0]	0	0	0
(0 1 1)[1 0 0]	0	45	90
(1 1 1)$[\bar{1}\,\bar{1}\,2]$	90	54.74	45

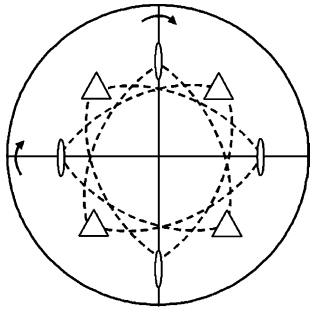

Fig. 8. Schematical drawing showing the main slip systems for explaining the two dominant rotations (see small arrows) occurring in the simulated nanoindent on the (0 0 1) oriented surface. The triangles indicate {1 1 1} slip plane normals and the elipses indicate ⟨1 1 0⟩ slip directions.

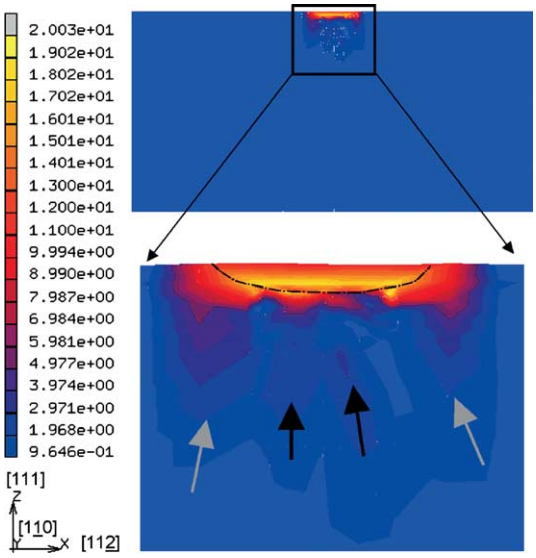

Fig. 9. Lateral distribution of the misorientation fields around and below the indent presented in the (1 $\bar{1}$ 0) crystallographic cutting plane. The indents were simulated on the (1 1 1) oriented surface plane of a copper single crystal using a conical indenter. The color code shows the accumulated orientation change in angles relative to the starting orientation. The re-orientation axis is not given. The dotted conus in the lower figure indicates the shape of the indenter.

dislocation loops typical of such indents indeed support the occurrence of at least two areas with larger re-orientation rates in the maximum shear zones around the indenter.

Related experimental work which aims at the 3D investigation of texture evolution below microindents in copper is currently being conducted by the group of

Yang et al. [34–36]. Our own experimental investigation of textures in the direct neighborhood of an indent provided only limited orientational information (Fig. 10). This is due to two facts. First, it is not possible to measure orientation changes directly inside the indents but only at their rims. Second, the plastic shear rates outside the indents are very small entailing only small re-orientation rates. This is exemplarily shown in Fig. 10 which gives an orientation mapping around an indent in the (0 0 1) crystal surface. The lateral step size of the microtexture mapping amounts to 100 nm. The color code indicates orientation changes relative to the undeformed crystal region far away from the indent using yellow for a maximum misorientation of 2°. Neither the pole figure of the experimental data (right hand side in Fig. 10) nor the texture mapping (left hand side in Fig. 10) reveal a clear symmetry or pronounced texture patterning as observed for the simulated textures.

4.3. Comparison of the simulated and experimentally obtained force–displacement curves

A comparison of the force–displacement curves between experiment and simulation reveal deviations above one order of magnitude, i.e. the data reveal very bad correspondence with each other even if the simulations would be artificially calibrated by help of the experimental results.

However, we must underline that experimental and simulated force–displacement curves are generally very difficult to compare. This is due to several reasons: first, our simulations were conducted for much larger indents when compared to the experiments. The reason for this is the finite treatment of tip curvature and contact. Second, the real tip function for the conical indenter as used in the experiments is difficult to measure and usually much sharper than that assumed in the finite element simulations. However, the tip radius function is an essential ingredient as a scaling factor to a finite element model. Using a tip function with a more realistic, i.e. with a very sharp curvature would not converge in a finite element simulation. This point must be regarded as the main reason for the deviation between experiment and simulation. Third, real conical tips are never perfectly conical as opposed to the tips assumed in the finite element model. Fourth, nanoindentation experiments are typically conducted using a force control approach whereas the simulated indents were conducted in a displacement-control mode. Fifth, there are substantial mesh effects. For instance, the simulated curve shows an irregular rather than a smooth course. Since our study concentrates on the orientation dependence of pile-up patterns we had to design an axially symmetrical mesh in order to minimize mesh effects with respect for pattern formation (Fig. 1). Such mesh type, however, is less suited for the simulation of force–displacement curves. When the symmetric indenter penetrates the sample switches between subsequent material elements which get in contact with the rigid indenter entail jumps in the response curve. Sixth, their could be an influence arising from the constitutive law we used for the indented material as outlined in Section 3.1. Seventh, the unknown frictional conditions might affect the predicted results.

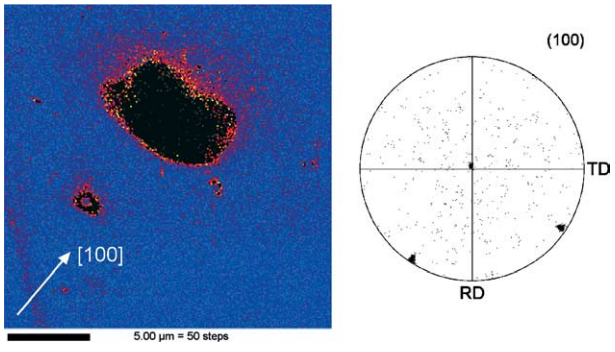

Fig. 10. Orientation mapping in the vicinity of the conical nanoindent on the (0 0 1) oriented copper surface (left hand side). The step size for the orientation mapping was 100 nm. The color code indicates orientation changes relative to the undeformed crystal region far away from the indent using yellow color for a maximum misorientation of 2°. Experimental pole figure of the scanned area (right hand side). (The sample is tilted as required by EBSD.)

5. Conclusions

We presented a study about the dependence of nanoindentation pile-up patterns and of local texture on the crystallographic orientation on copper single crystals. We used a conical indenter in order to avoid symmetries others than those of the crystal structure. Texture measurements around the indents were conducted by use of a high resolution EBSD technique. The experiments were complemented by corresponding simulations which were conducted by means of a 3D elastic–viscoplastic crystal plasticity finite element method which takes full account of crystallographic slip and orientation changes during indentation. The main conclusions are:

- The pile-up patterns depend strongly on the crystallographic orientation of the indented surface. Patterns on the surfaces of (0 0 1)-, (0 1 1)- and (1 1 1)-oriented copper single crystals have four-, two-, and sixfold symmetry, respectively.
- The patterns can be very well simulated by using a 3D elastic–viscoplastic crystal-plasticity finite element method.
- The patterns can be kinematically explained in terms of the pronounced out-of-plane displacement of material along the intersection vectors between the primary crystallographic slip planes and the indented surface planes.

- The patterns cannot be interpreted in terms of conventional global isotropic strain-hardening criteria since local crystallographic criteria seem to prevail.
- The fact that all patterns are pile-up rather than sink-in patterns is attributed to the highly crystallographic and localized flow of material only along small volumes. We conclude that in these confined zones only little microscopic strain hardening occurs due to parallel slip promoting pile-up instead of sink-in behavior.

Acknowledgements

Helpful comments of Prof. P.-L. Larsson of the Royal Institute of Technology, Sweden, of Dr. Z. Zhao at MIT, USA, and of Prof. W.D. Nix at Stanford, USA, are gratefully acknowledged.

References

[1] Pharr GM, Oliver WC, Brotzen FR. J Mater Res 1992;7:613.
[2] Nix WD. Mater Sci Eng A 1997;234–236:37.
[3] Chaudhri MM, Winter M. J Phys D – Appl Phys 1988;21:370.
[4] Alcala J, Barone AC, Anglada M. Acta Mater 2000;48:3451.
[5] Flom DG, Komanduri R. Wear 2002;252:401.
[6] Hollatz M, Bobeth M, Pompe W, Marx V. Acta Mater 1996;44:4149.
[7] Tymiak NI, Kramer DE, Bahr DF, Wyrobek TJ, Gerberich WW. Acta Mater 2001;49:1021.
[8] Bahr DF, Kramer DE, Gerberich WW. Acta Mater 1998;46:3605.
[9] Gouldstone A, Koh H-J, Zeng K-Y, Giannakopoulos AE, Suresh S. Acta Mater 2000;48:29.
[10] Gaillard Y, Tromas C, Woirgard J. Acta Mater 2003;51:1059.
[11] Li J, Van Vliet K, Ting Z, Yip S, Suresh S. Nature 2002;418:307.
[12] Van Vliet K, Li J, Ting Z, Yip S, Suresh S. Phys Rev B 2003;67:104105.
[13] Kalidindi SR, Schoenfeld SE. Mater Sci Eng A 2000;293:120.
[14] Arsenlis A, Parks DM. J Mech Phys Solids 2002;50:1979.
[15] Kalidindi SR, Anand L. Metall Trans A 1993;24:989.
[16] Kalidindi SR, Bronkhorst CA, Anand L. J Mech Phys Solids 1992;40:537.
[17] Lee EH. J Appl Mech 1969;36:1.
[18] Rice JR. J Mech Phys Solids 1971;19:433.
[19] Hill R, Rice JR. J Appl Mech 1972;20:401.
[20] Asaro RJ, Rice JR. J Appl Mech 1977;25:309.
[21] Peirce D, Asaro RJ, Needleman A. Acta Metall 1982;30:2037.
[22] Asaro RJ, Needleman A. Acta Metall 1985;33:923.
[23] MSC. Marc user's manual, vol. D, MSC Software Corporation, 2001.
[24] Verleene A, Dubar L, Dubois A, Dubar M, Oudin J. Int J Plast 2002;18:997.
[25] Montmitonnet P, Edlinger ML, Felder E. J Tribol, Trans ASME 1993;115:10.
[26] Raabe D, Sachtleber M, Zhao Z, Roters F, Zaefferer S. Acta Mater 2001;49:3433.
[27] Dève H, Harren SV, McCullough C, Asaro RJ. Acta Mater 1988;36:341.
[28] Harren SV, Asaro RJ. J Mech Phys Solids 1989;37:191.
[29] McElhaney KW, Vlassak JJ, Nix WD. J Mater Res 1998;13:1300.
[30] Lim YY, Chaudhri MM. Phil Mag A 1999;79:2979.
[31] Lim YY, Chaudhri MM. Phys Stat Sol A 2002;194:19.
[32] Lim YY, Chaudhri MM. Phil Mag A 2002;82:2071.
[33] Lui Y, Ngan AHW. Scripta Mater 2001;44:237.
[34] Yang W, Larson BC, Pharr GM, Ice GE, Swadener JG, Budai JD, et al. Material Research Society Symposium Proceedings, vol. 750, 2003, Y.8.26.1.
[35] Larson BC, Yang W, Ice GE, Swadener JG, Budai JD, Tischler JZ. Nature 2002;415:887.
[36] Yang W, Larson BC, Pharr GM, Ice GE, Swadener JG, Budai JD, et al. Material Research Society Symposium Proceedings, vol. 779, 2003, W.5.34.1.